# Energy limit in cyclotron autoresonance acceleration

Changbiao Wang and J. L. Hirshfield
*Omega-P, Inc., 2008 Yale Station, New Haven, Connecticut 06520*
*and Physics Department, Yale University, New Haven, Connecticut 06511*
(Received 19 October 1994)

A multimegawatt gyroharmonic converter depends critically on the parameters of a spatiotemporally modulated gyrating electron beam prepared using a cyclotron autoresonance accelerator (CARA). This paper extends a prior analysis of CARA [B. Hafizi, P. Sprangle, and J. L. Hirshfield, Phys. Rev. E **50**, 3077 (1994)] to identify an approximate constant of the motion and, therefore, to give limits to the beam energy from CARA that can be utilized in a harmonic converter. It is also shown that particles are strongly phase trapped during acceleration in CARA and thus are insensitive to deviations from exact autoresonance. This fact could simplify construction of the up-tapered guide magnetic field in the device and augurs well for production of high-quality multimegawatt beams using CARA.

PACS number(s): 29.17.+w, 29.27.−a, 41.75.−i, 52.75.Ms

## I. INTRODUCTION

Considerable effort has been devoted in the past few years to the study of gyroharmonic conversion [1–4] for the production of multimegawatt rf power at cm wavelengths, where advanced klystrons may not be suitable as drivers for future linear colliders. Gyroharmonic conversion depends on the efficient acceleration of an electron beam using a low frequency rf driver (a SLAC klystron at 2.856 GHz, for example), with subsequent highly preferential generation of power at a harmonic of the driver (14.28 GHz in experiments underway at Yale University). Particle simulation studies have shown that the conversion process can have a high transverse efficiency, with only small portions of the beam power driving competing modes at frequencies other than the design frequency. Moreover, the spent beam particles are left, after saturation, nearly all at the same energy and gyration phase; this suggests that a single-stage depressed collector or second-stage converter can be used to yield very high efficiency beam energy utilization.

The above conclusions for the converter assume that a means exists for efficient production of a high quality spatiotemporally modulated gyrating electron beam. Such a means appear to be cyclotron autoresonance acceleration (CARA), wherein gyrating electrons are maintained in phase synchronism with a rotating $TE_{11}$ waveguide field using tapers in magnetic field and/or waveguide radius. Work to date on this acceleration mechanism [5–7] has shown that nearly all the applied rf power can be converted to beam kinetic energy when the tapers are appropriately chosen, but that there is an upper limit to the energy gain that can be imparted to a beam. Studies of the evolution of beam quality have shown that there is little degradation in beam emittance during the CARA process, provided one does not work too close to the upper energy limit of the device [6].

In this paper, it is shown that the maximum limit to energy in a CARA found empirically in prior work can be confirmed analytically. This is possible because an approximate constant of the motion has been identified from the basic governing equations. When this constant of the motion is combined with conditions required for the beam at the entrance to the harmonic converter section, a very simple upper limit is found for the energy of a beam produced by a CARA that is usable in a harmonic converter. Such a result is helpful in scaling harmonic converters to power levels that are required in future linear colliders.

One criticism of CARA that has been expressed [7] is that maintenance of synchronism between particles and the rf drive wave requires construction of a magnetic field taper with very high precision. Otherwise, it has been suggested, the particles will not remain in resonance, and beam quality will degenerate. Results of study of this point are reported here, wherein it is shown that large deviations from the exact autoresonant condition can occur, through deviations in guide magnetic field from the resonant profile, without materially affecting the acceleration or beam quality. This occurs because particles are strongly trapped in moving potential buckets that insure phase synchronism even when the exact autoresonance condition is violated. This realization should simplify the practical construction of a CARA for production of high quality beams needed in harmonic converters.

## II. BASIC EQUATIONS AND MAXIMUM ACCELERATION ENERGY

In this section, we present self-consistent basic equations that describe the interaction of an electron beam with the rf field in CARA. An idealized diagram of CARA is shown in Fig. 1. The dynamic equations follow from the Lorentz force equation by making some assumptions, and rf pump depletion is included by conservation of energy. From these equations, we will derive an approximate constant of motion, which leads to the maximum acceleration energy that can be reached in an ideal CARA.

Suppose that the CARA employs a rotating $TE_{11}$ mode

 

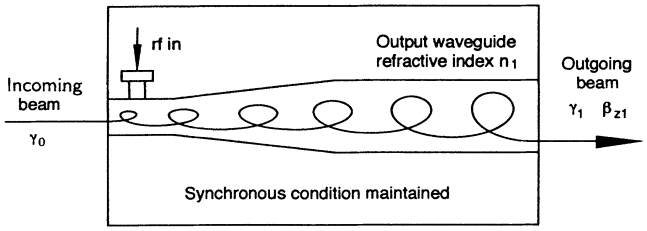


FIG. 1. Diagram of an idealized $TE_{11}$-mode CARA.

in a cylindrical waveguide. In a cylindrical coordinate system $(r,\varphi,z)$, the rf magnetic fields are given by

$$B_r=b_{\rm rf}\frac{k_z}{k_c}J_1'(k_cr)\sin(\chi-\varphi)\ , \tag{1}$$

$$B_\varphi=-b_{\rm rf}\frac{k_z}{k_c}\frac{1}{k_cr}J_1(k_cr)\cos(\chi-\varphi)\ , \tag{2}$$

$$B_z=b_{\rm rf}J_1(k_cr)\cos(\chi-\varphi)\ , \tag{3}$$

where $k_z$ is the wave number, $k_c$ is the cutoff wave number, $b_{\rm rf}$ is the amplitude, $J_1(\xi)$ is the first kind of Bessel function of the first order, $J_1'(\xi)\equiv(d/d\xi)J_1(\xi)$, and $\chi=\omega t-\int_0^z k_z dz$ with $\omega$ the rf field frequency. The rf electric fields are related by $E_r=B_\varphi\omega/k_z$ and $E_\varphi=-B_r\omega/k_z$. The applied dc axisymmetric magnetic field is given by

$$\mathbf{B}_{\rm static}(\mathbf{x})\approx B_0(z)\mathbf{e}_z-\frac{1}{2}\frac{dB_0(z)}{dz}r\mathbf{e}_r\ , \tag{4}$$

and the electron gyration frequency is defined by $\Omega_0=eB_0(z)/m$, where $e$ is the magnitude of the electron charge and $m$ is the rest mass.

In velocity space, the variable change between Cartesian and cylindrical coordinate systems is given by $\beta_x=\beta_\perp\cos\theta$, $\beta_y=\beta_\perp\sin\theta$, and $\beta_z=\beta_z$, where $\beta_i$ ($i\equiv x$, $y$, $z$, and $\perp$) denotes a component of the electron velocity normalized to the light speed $c$ in free space. When assumptions of zero guiding center spread and zero guiding center drift are made, the equations of motion of electrons in the CARA were given by Hafizi, Sprangle, and Hirshfield [6]. In this work, we further assume that the wave number shift $\Delta k$ is much less than $n$ and the pump depletion rate $\Gamma$ is much less than $1-n\beta_z$, where $\Gamma$ and $\Delta k$ are defined in Ref. [6], and $n=k_zc/\omega$ is the refractive index. Accordingly, the equations of motion can be further simplified to become

$$\frac{du_\perp}{d\xi}=2b(\xi)J_1'(k_c\rho)\frac{(1-n\beta_z)}{\beta_z}\cos\psi+\frac{u_\perp}{2b_0}\frac{db_0}{d\xi}\ , \tag{5}$$

$$\frac{du_z}{d\xi}=2b(\xi)J_1'(k_c\rho)\frac{u_\perp}{u_z}n\cos\psi-\frac{u_\perp^2}{2u_zb_0}\frac{db_0}{d\xi}\ , \tag{6}$$

$$\frac{d\psi}{d\xi}=\Delta-2b(\xi)J_1(k_c\rho)\frac{1}{\beta_z}\left[\frac{(1-n\beta_z)}{u_\perp k_c\rho}-\frac{ck_c}{\gamma\omega}\right]\sin\psi\ , \tag{7}$$

where $u_\perp=\gamma\beta_\perp$, $u_z=\gamma\beta_z$, $\psi=\theta-\chi$, $\zeta=z\omega/c$, $\gamma=(1+u_\perp^2+u_z^2)^{1/2}$ is the relativistic factor, $\rho=u_\perp c/\Omega_0$ is the electron gyration radius, $\Delta=(\Omega_0/\gamma-\omega+k_zc\beta_z)/(\omega\beta_z)$ is the relative frequency detuning, $b_0=\Omega_0/\omega$, and $b(\zeta)=eb_{\rm rf}(\zeta)/[2mck_c(\zeta)]$. In the above equations, the refractive index $n$ is equivalent to the mode's normalized group velocity $v_{\rm gr}/c$, where $v_{\rm gr}=d\omega/dk_z$, and $\psi$ stands for the angle between an electron and the rf field. If $\psi=0$, the direction of the electron motion is opposite to the electric field and the electron is accelerated most effectively.

Suppose that there is no power reflection in the waveguide. Conservation of energy then requires that

$$P_{\rm rf}(\zeta)=P_{\rm rf0}+P_{b0}-I\frac{mc^2}{e}\frac{1}{N}\sum_{i=1}^{N}[\gamma_i(\zeta)-1]\ , \tag{8}$$

where $P_{\rm rf}$ is the rf pump power, $P_{\rm rf0}$ and $P_{b0}$ are, respectively, the initial rf and beam powers, $I$ is the beam current, and $N$ is the total computational particle number. Equation (8) relates Eqs. (1)–(3) to Eqs. (5)–(7) with energy self-consistence through the following equation:

$$b_{\rm rf}(\zeta)=\left[\frac{2k_c^4(\zeta)}{\pi c^2k_z(\zeta)\varepsilon_0\omega}\frac{P_{\rm rf}(\zeta)}{(\nu_{11}^2-1)J_1^2(\nu_{11})}\right]^{1/2}\ , \tag{9}$$

where $\nu_{11}=1.841$ is the first root of $J_1'(\xi)=0$. In this calculational model, compared with that in Ref. [6], the influence of the electron beam on the refractive index is ignored. Pump depletion is directly included in the coefficient $b(\zeta)$ of Eqs. (5)–(7) through conservation of energy.

Eqs. (1)–(3), (5)–(7), and (8) are the basic equations needed in the following analysis and calculation. The Lorentz force equation, which has six component equations, here has been simplified into three equations [Eqs. (5)–(7)]. However, the results from the three and six equations are almost the same, as shown in Fig. 2 for a sample electron. For this example, the applied axial magnetic field and the waveguide are uniform. Hence this electron cannot keep synchronous with the rf field, and it goes back to its initial state after a synchronous oscillation period (six gyration periods). The close agreement between the solution of the approximate three-equation system and the exact six-equation system is apparent.

From Eqs. (5) and (6), we obtain

$$\frac{d}{d\zeta}\left[\frac{u_\perp^2}{b_0}\right]=\frac{2u_\perp}{b_0}2bJ_1'(k_c\rho)\frac{(1-n\beta_z)}{\beta_z}\cos\psi\ , \tag{10}$$

$$\frac{d\gamma}{d\zeta}=2bJ_1'(k_c\rho)\frac{u_\perp}{u_z}\cos\psi\ . \tag{11}$$

Substituting Eq. (11) into Eq. (10) yields

$$\frac{d}{d\zeta}\left[\frac{u_\perp^2}{b_0}\right]=2\frac{\gamma(1-n\beta_z)}{b_0}\frac{d\gamma}{d\zeta}\ . \tag{12}$$

We assume that in an ideal CARA the synchronous condition

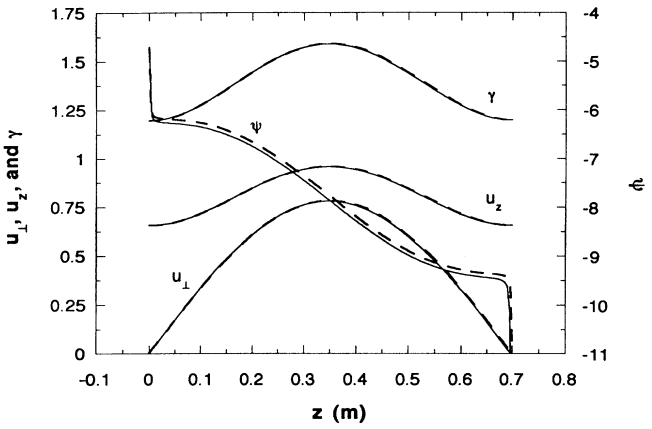


FIG. 2. Comparison between the results from three equations and six equations, respectively. For a sample electron, the applied axial magnetic field and the waveguide are uniform. Solid line: three equations, and dashed line: six equations.

$$\omega - k_z c\beta_z - \frac{\Omega_0}{\gamma} = 0 \quad \text{or} \quad b_0 = \gamma(1 - n\beta_z) \tag{13}$$

is maintained. From this we obtain a constant of motion for synchronous particles,

$$\frac{u_\perp^2}{b_0} - 2\gamma = \text{const} . \tag{14}$$

It should be noted that this is not an exact constant of motion because it neglects refractive effects of the beam, and higher order terms for nonsynchronous particles in the exact equations that arise from pump depletion. Furthermore, a magnetic field must satisfy $\nabla \cdot \mathbf{B} = 0$ and $\nabla \times \mathbf{B} = 0$, but the one required to maintain Eq. (13) may not. Moreover, different electrons with different initial conditions may have different required resonant fields. However, simulations indicate that the left-hand side of Eq. (14) changes very little when the applied magnetic field is close to that for the average particle. A constant of motion of this form has been derived for cyclotron resonance masers [8], and was employed in the context of microwave heating of plasmas without pump depletion taken into account [9,10].

For an ideal single-momentum electron beam, the initial transverse velocity should be zero. In such a case, Eq. (14) becomes

$$\frac{u_\perp^2}{b_0} = 2(\gamma - \gamma_0) , \tag{15}$$

where $\gamma_0$ is the beam's initial relativistic factor. Substituting Eq. (13) into Eq. (15), we obtain

$$\gamma_1 = \frac{\gamma_0(1 - n_1\beta_{z1}) \pm [\gamma_0^2(1 - n_1\beta_{z1})^2 - (1 - 2n_1\beta_{z1} + \beta_{z1}^2)]^{1/2}}{1 - 2n_1\beta_{z1} + \beta_{z1}^2} \qquad (\gamma_1 > \gamma_0) , \tag{16}$$

where $\gamma_1$, $\beta_{z1}$, and $n_1$ denote the output parameters for an ideal $TE_{11}$-mode CARA, as shown in Fig. 1.

Equation (16) gives the complete dependence of $\gamma_1$ on $\beta_{z1}$ at the exit of a CARA with output waveguide refractive index $n_1$ and initial beam energy $\gamma_0$, no matter how the magnetic field or waveguide radius are tapered for synchronism, and no matter how much rf power is used. Equation (16) can be used to estimate CARA parameters without solving differential equations. As a comparison, we calculated Eq. (16) using the parameters $\gamma_0 = 1.1957$ (100 kV) and $n_1 = 0.7677$, 0.9373, and 0.9979, which were examples taken in Ref. [6]. As shown in Fig. 3, the maximum relativistic factors are, respectively, 2.22, 3.08, and 11.32, very close to the results 2.17, 2.96, and 10.78 found in Ref. [6]. It should be noted that the maximum $\gamma = 2.17$ case of Ref. [6] corresponds to about 80% extraction of rf power, so that the pump is significantly depleted.

From Fig. 3, we can find that for a given $\gamma_1$ (except for the maximum $\gamma_1$) there are two values of $\beta_{z1}$ on each curve. The right branch of a curve is for a beam with an initial energy of $\gamma_0$ and zero-initial transverse velocity, while the left branch is for another initially modulated beam with an initial energy of $\gamma_0 + (\gamma_0^2 - 1)^{1/2}$ and zero-initial axial velocity, which is of less practical interest. In fact, if we use the initial energy $\gamma_0 + (\gamma_0^2 - 1)^{1/2}$ and zero-initial axial velocity to insert into Eq. (14), then we retrieve Eq. (15). The two beams have the same maximum acceleration energy.

An alternative expression for Eq. (16) is given by

$$\beta_{z1} = \frac{1}{\gamma_1}[n_1(\gamma_1 - \gamma_0) \pm D^{1/2}] \quad (\gamma_1 > \gamma_0,\ \beta_{z1} > 0) , \tag{17}$$

where $D = (\gamma_0^2 - 1) - (1 - n_1^2)(\gamma_1 - \gamma_0)^2$. From $D \geq 0$, we obtain

$$\gamma_0 \leq \gamma_1 \leq \gamma_{1\,\max} , \tag{18}$$

where the maximum acceleration energy is given by

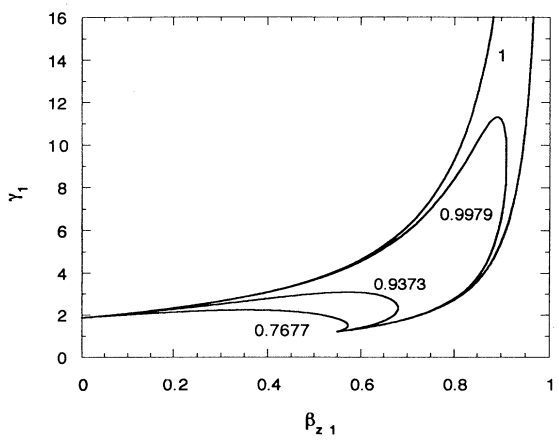


FIG. 3. Dependence of outgoing-beam relativistic factor $\gamma_1$ on normalized axial velocity $\beta_{z1}$ for different refractive index $n_1$. The initial beam energy is 100 kV ($\gamma_0 = 1.1957$). $\gamma_{1\,\max} = 2.22$ for $n_1 = 0.7677$, $\gamma_{1\,\max} = 3.08$ for $n_1 = 0.9373$, $\gamma_{1\,\max} = 11.32$ for $n_1 = 0.9979$, and $\gamma_{1\,\max} = +\infty$ for $n_1 = 1$.

$$\gamma_{1\max}=\gamma_0+\left[\frac{\gamma_0^2-1}{1-n_1^2}\right]^{1/2} . \tag{19}$$

From Eq. (17) again we obtain the axial velocity corresponding to the maximum acceleration energy, that is,

$$\beta_{z1\max}=n_1\left[1-\frac{\gamma_0}{\gamma_{1\max}}\right] . \tag{20}$$

Substituting Eqs. (19) and (20) into Eq. (13) yields the corresponding axial magnetic field

$$B_{01\max}=\frac{m}{e}\omega\{\gamma_0+[(1-n_1^2)(\gamma_0^2-1)]^{1/2}\} . \tag{21}$$

Formulas similar to Eqs. (19) and (21) were obtained by Voronin and Kononov, based on the model of a circularly polarized plane wave without pump depletion or wavenumber tapering taken into account [11].

From Eq. (19), one sees that the maximum limit to acceleration energy in a CARA depends only on the initial beam energy and the output waveguide refractive index, provided power depletion is less than total. Figure 4 shows the dependence of maximum acceleration energy $\gamma_{1\max}$ on index $n_1$ for beams with different initial energy. Indeed, as suggested in [6], Fig. 4 shows that CARA behaves approximately like a $\gamma$ doubler for a wide range of index, except for $n_1$ close to 1.

In the limit of weak dispersion where the normalized phase velocity $\beta_p$ $(=1/n)$ is approximately equal to unity, the maximum acceleration gain is given by

$$G\equiv\frac{\gamma_{1\max}-\gamma_0}{\gamma_0-1}=\left[\frac{\gamma_0+1}{2(\gamma_0-1)}\right]^{1/2}\frac{1}{(\beta_p-1)^{1/2}} . \tag{22}$$

The factor $(\beta_p-1)^{-1/2}$ in the above equation was empirically obtained by Chen [5]. Taking $\gamma_0=1.15$ and $\beta_p=1.01$, we have $G=26.8$, a little larger than the result 26.1 found by Chen. The difference might be caused by the nonzero initial transverse velocity in his example.

When the nonzero initial transverse velocity is taken into account, the maximum acceleration energy can be written as

$$\gamma_{1\max}=\gamma_0\gamma_d+\left[\frac{\gamma_0^2\gamma_d^2-1}{1-n_1^2}\right]^{1/2} , \tag{23}$$

where

$$\gamma_d=1-\frac{\beta_{\perp 0}^2}{2(1-n_0\beta_{z0})} . \tag{24}$$

Here $\beta_{\perp 0}$ and $\beta_{z0}$ are, respectively, the initial transverse and axial normalized velocities, and $n_0$ is the refractive index at the CARA entrance. From Eq. (24) we find that $0.5(1+1/\gamma_0^2)\le\gamma_d\le 1$ and $\gamma_d=1$ when $\beta_{\perp 0}=0$. Hence an electron beam with a zero-initial transverse velocity has the largest maximum acceleration energy.

For $\gamma_d\approx 1$, Eq. (22) can be modified as

$$G=\left[\frac{\gamma_0^2\gamma_d^2-1}{2(\gamma_0-1)^2}\right]^{1/2}\frac{1}{(\beta_p-1)^{1/2}} . \tag{25}$$

Again, taking Chen's example where $\gamma_0=1.15$, $\beta_p=1.01$, and $\beta_{\perp 0}/\beta_{z0}=0.2$, we have $\gamma_d=0.9910$ and $G=25.8$, which is closer to 26.1 than the prior value of 26.8.

Next let us examine separately how to accelerate an electron beam in a CARA either with a constant waveguide radius (tapering the magnetic field), or a constant axial magnetic field (tapering the waveguide radius). Suppose that the beam has no initial transverse velocity. From Eqs. (13) and (15), we obtain dependence of normalized energy $\gamma$ on normalized axial magnetic field $b_0$, that is,

$$\gamma=b_0+\left\{\frac{n_0^2}{1-n_0^2}[(\gamma_0^2-1)-(\gamma_0-b_0)^2]\right\}^{1/2}$$

(tapering the magnetic field) (26)

where $\gamma_0-n_0(\gamma_0^2-1)^{1/2}\le b_0\le\gamma_0+[(\gamma_0^2-1)(1-n_0^2)]^{1/2}$. When the normalized axial magnetic field $b_0$ reaches $\gamma_0+[(\gamma_0^2-1)(1-n_0^2)]^{1/2}$, the transverse magnetic field rises steeply and the axial velocity of those electrons at that plane becomes zero and reverses, resulting in termination of acceleration. Obviously, the maximum acceleration energy is the same as the one given by Eq. (19) by setting $n_1=n_0$.

Similarly, we can obtain dependence of normalized energy $\gamma$ on waveguide refractive index $n$, that is,

$$\gamma=\gamma_0+n_0(\gamma_0^2-1)^{1/2}\left[\frac{n}{n_0}\left[\frac{1-n_0^2}{1-n^2}\right]^{1/2}-1\right]$$

(tapering the waveguide radius) (27)

where $n_0\le n<1$. From the above, we find that there is no energy limit for a tapered waveguide-radius CARA if there is no limit to the radius. However, the waveguide radius in a CARA must be finite in practice. Hence for such a finite radius CARA, the maximum acceleration energy is given by

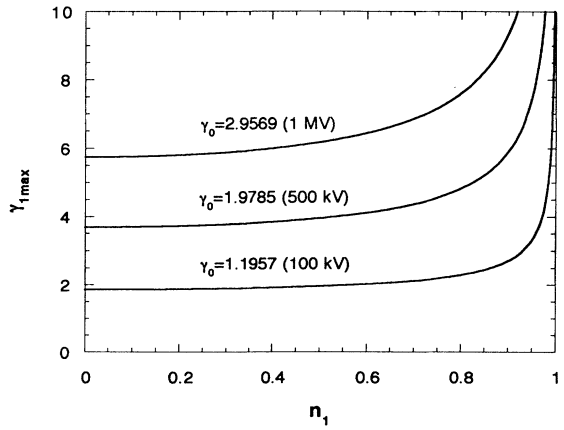


FIG. 4. Dependence of maximum acceleration energy $\gamma_{1\max}$ on output waveguide refractive index $n_1$ for different initial beam energy. In a wide range of index, the CARA behaves like a $\gamma$ doubler [6].

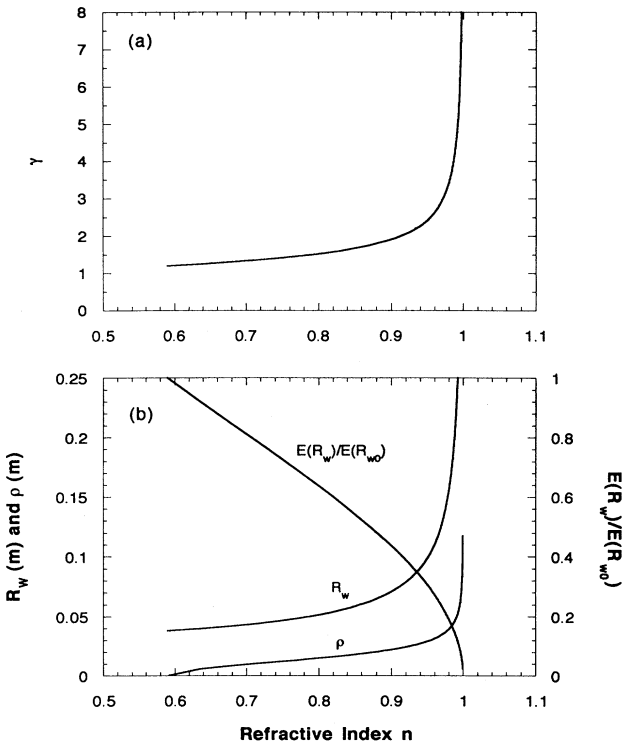


FIG. 5. Dependence of (a) acceleration energy $\gamma$, and (b) waveguide radius $R_w$, gyration radius $\rho$, and empty-waveguide relative electric field amplitude $E(R_w)/E(R_{w0})$ on refractive index $n$ for a tapered waveguide-radius CARA with initial radius $R_{w0}=3.81$ cm and $\gamma_0=1.1957$ (100 kV).

$$\gamma_{1\max}=\gamma_0+n_1\left[\frac{\gamma_0^2-1}{1-n_1^2}\right]^{1/2}$$

(tapering the waveguide radius) . (28)

Comparing Eqs. (19) and (28), we see that for given $\gamma_0$ and $n_1$ the tapered magnetic-field CARA has a larger maximum acceleration energy.

Figure 5 shows dependence of acceleration energy $\gamma$, waveguide radius $R_w$, gyration radius $\rho$, and empty-waveguide relative electric field amplitude $E(R_w)/E(R_{w0})$ on refractive index $n$ for a tapered waveguide-radius CARA with initial radius $R_{w0}=3.81$ cm and $\gamma_0=1.1957$ (100 kV). From it we find that the waveguide radius greatly increases for large acceleration energy, which leads to rapid decrease in acceleration gradient. For example, when $\gamma$ is accelerated to 4.0 from 2.0, $R_w$ increases to 18.8 cm from 7.6 cm, and $E(R_w)/E(R_{w0})$ decreases to 15.7% from 40.5%. It is interesting, however, to note that the gyration radius is always smaller than the waveguide radius in the tapered waveguide-radius CARA.

## III. SOME BASIC PARAMETERS FOR A HARMONIC CONVERTER

The gyroharmonic converter utilizes a spatiotemporally modulated electron beam prepared by a CARA. Although Eq. (16) establishes all possible dependences of acceleration energy on axial velocity for the CARA, not all the electron beams with the parameters given by the equation can be used to generate coherent harmonic radiation in a converter. In this section, we will derive a criterion that a beam from a CARA has to satisfy for the converter, and give some typical parameters for the Yale CARA.

As mentioned previously, the beam from a CARA satisfies the synchronous condition

$$\omega-k_{z1}c\beta_{z1}-\frac{\Omega_{01}}{\gamma_1}=0 \quad \text{or} \quad \Omega_{01}=\omega\gamma_1(1-n_1\beta_{z1}) . \tag{29}$$

Here and below, a quantity with the subscript 1 refers to the CARA exit. From the above we obtain the required resonant magnetic field

$$B_{01}=\frac{m}{e}\omega\gamma_1(1-n_1\beta_{z1}) . \tag{30}$$

The ratio of transverse velocity to axial velocity at the CARA exit is given by

$$\alpha_1=\frac{1}{\beta_{z1}}\left[1-\frac{1}{\gamma_1^2}-\beta_{z1}^2\right]^{1/2} . \tag{31}$$

To generate coherent harmonic output, the beam at the entrance to the harmonic converter section has to fulfill both the synchronous and the grazing conditions [1]:

$$l\omega-k_{z2}c\beta_{z2}-\frac{l\Omega_{02}}{\gamma_2}=0 \quad \text{or} \quad \Omega_{02}=\omega\gamma_2(1-n_2\beta_{z2}) , \tag{32}$$

$$n_2=\beta_{z2} \quad \text{(grazing condition)} , \tag{33}$$

where $l$ is the harmonic index. In the above equations and below, a quantity with the subscript 2 refers to the harmonic converter section entrance. Equation (33) signifies that the empty-waveguide dispersion curve is tangent to the line described by Eq. (32).

To realize a transition from the CARA exit to the harmonic converter section entrance, an rf absorbing drift tube is inserted (see Fig. 10). In the drift tube, there is no rf field and $\gamma_1=\gamma_2$, but the magnetic field taper continues. From Eq. (12), we know that $u_\perp^2/b_0$ is also a constant (adiabatic invariant) so that we have

$$\frac{\Omega_{02}}{\Omega_{01}}=\frac{1-\frac{1}{\gamma_1^2}-\beta_{z2}^2}{1-\frac{1}{\gamma_1^2}-\beta_{z1}^2} . \tag{34}$$

Comparing Eqs. (29), and (32)–(34), we obtain

$$\beta_{z2}=\left[\frac{\gamma_1^2\beta_{z1}(\beta_{z1}-n_1)+n_1\beta_{z1}}{\gamma_1^2\beta_{z1}(\beta_{z1}-n_1)+1}\right]^{1/2} . \tag{35}$$

Substituting Eq. (15) into Eq. (35), we obtain

$$\beta_{z2}=\left[\frac{\gamma_1(2\gamma_0-\gamma_1)-1}{\gamma_1(2\gamma_0-\gamma_1)}\right]^{1/2} . \tag{36}$$

A necessary condition that there exists a solution to Eq. (35) or Eq. (36) is that the inequality

$$\beta_{z1} > n_1 \left[1-\frac{1}{\gamma_1^2}\right] \quad \text{or} \quad \gamma_1(2\gamma_0-\gamma_1)>1 \tag{37}$$

must hold. From this it follows that only when an electron beam out of a CARA satisfies the above condition, the beam may satisfy both the synchronous and grazing conditions for harmonic radiation after it passes the drift tube. This condition puts a limit to the usable acceleration energy of a beam from the CARA. From Eq. (37), we can directly obtain the usable acceleration energy upper limit

$$\gamma_{1\,\text{limit}} = \gamma_0 + (\gamma_0^2-1)^{1/2}\,, \tag{38}$$

which corresponds to a usable acceleration voltage limit,

$$V_{1\,\text{limit}} = V_0 + V_0\left[1+\frac{2mc^2}{eV_0}\right]^{1/2}, \tag{39}$$

with $V_0$ the beam's initial voltage. For $V_0$=(100, 250, 500 kV), $V_{1\,\text{limit}}$=(435, 814, 1372 kV). Similarly, we can obtain

$$B_{02} = \frac{m}{e}\frac{\omega}{2\gamma_0-\gamma_1} \quad \text{and} \quad \alpha_2 = \left[\frac{2(\gamma_1-\gamma_0)}{\gamma_1[\gamma_1(2\gamma_0-\gamma_1)-1]}\right]^{1/2}. \tag{40}$$

Inequality (37) is a criterion which an electron beam from the CARA has to meet for a converter, and Eq. (38) shows the usable acceleration energy limit of the beam. Equations (30), (31), (36), and (40) give dependence of $B_{01}$, $\alpha_1$, $\beta_{z2}$, $B_{02}$, and $\alpha_2$ on $\gamma_1$. It should be noted that the refractive index $n_1$ does not appear in expressions for $\beta_{z2}$, $B_{02}$, and $\alpha_2$. From these formulas we can make a rough estimation of these basic parameters.

Following is a numerical example that applies to the Yale CARA. Therefore, let us take $\gamma_0$=1.1957 (100 kV) and $n_1$=0.795 85 at 2.856 GHz. As shown in Fig. 6, the

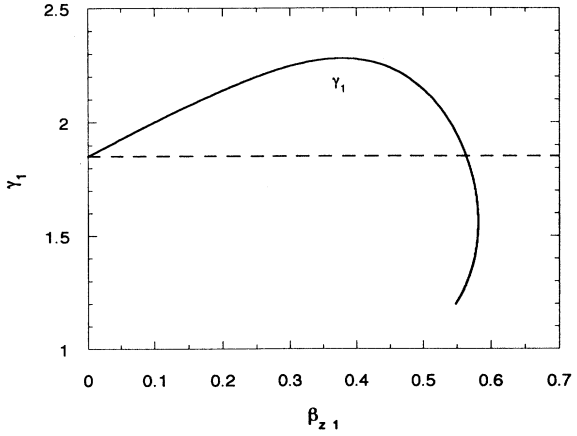


FIG. 6. Dependence of outgoing-beam normalized energy $\gamma_1$ on normalized axial velocity $\beta_{z1}$. $\gamma_0$=1.1957 and $n_1$=0.795 85. Only the part of curve $\gamma_1$ below the dashed line for $\gamma_1$=1.8512 is usable for a converter. At $\beta_{z1}$=0.5714, $\gamma_1$=1.7782.

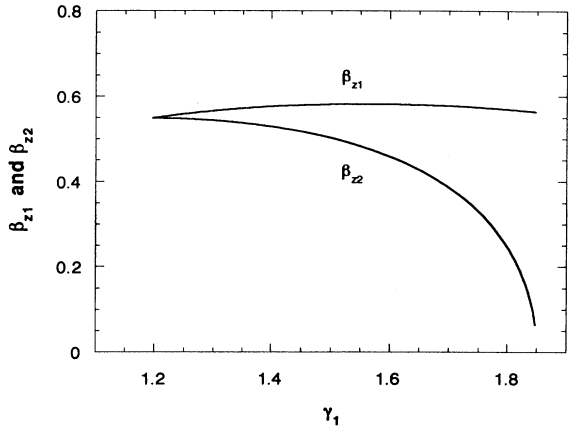


FIG. 7. Dependence of axial velocities $\beta_{z1}$ and $\beta_{z2}$ ($=n_2$) on $\gamma_1$. $\gamma_0$=1.1957 and $n_1$=0.795 85. $\beta_{z2}$ decreases rapidly with $\gamma_1$ approaching the usable acceleration energy limit, but $\beta_{z1}$ does not change very much. At $\gamma_1$=1.7782, $\beta_{z2}$=0.2878.

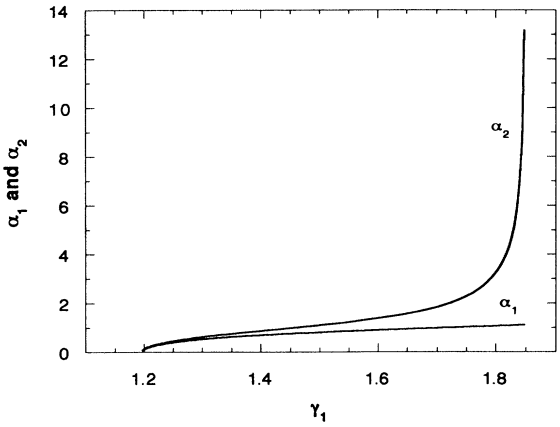


FIG. 8. Dependence of velocity ratios $\alpha_1$ and $\alpha_2$ on $\gamma_1$. $\gamma_0$=1.1957 and $n_1$=0.795 85. $\alpha_2$ increases steeply with $\gamma_1$ approaching the usable acceleration energy limit At $\gamma_1$=1.7782, $\alpha_1$=1.0460, and $\alpha_2$=2.6932.

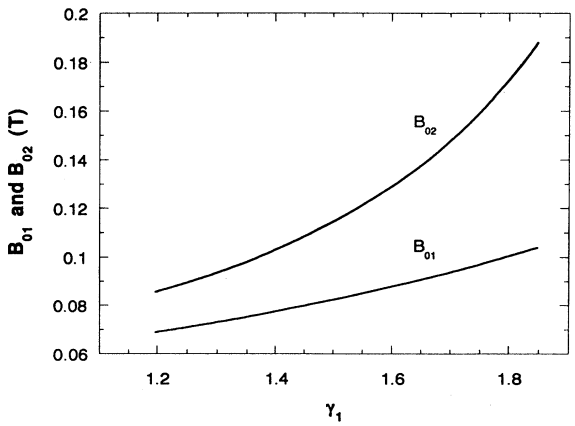


FIG. 9. Dependence of axial magnetic fields $B_{01}$ and $B_{02}$ on $\gamma_1$. $\gamma_0$=1.1957 and $n_1$=0.795 85. $B_{02}$ increases faster with $\gamma_1$ than $B_{01}$. At $\gamma_1$=1.7782, $B_{01}$=0.0989 T and $B_{02}$=0.1664 T.

dashed line $\gamma_1=\gamma_0+(\gamma_0^2-1)^{1/2}=1.8512$ and curve $\gamma_1$ [from Eq. (16)] has two intersection points, with one of them at $\beta_{z1}=0$. The line divides the curve into two parts, and only the part below the line is usable for a converter. Figure 7 shows dependence $\beta_{z1}$ and $\beta_{z2}$ on $\gamma_1$, Fig. 8 shows dependence of $\alpha_1$ and $\alpha_2$ on $\gamma_1$, and Fig. 9 shows dependence of $B_{01}$ and $B_{02}$ on $\gamma_1$. From these figures we find that a larger acceleration energy $\gamma_1$ results in a smaller axial velocity $\beta_{z2}$ and a larger velocity ratio $\alpha_2$, although $\beta_{z1}$ does not change very much. The required magnetic field $B_{02}$ also increases with the acceleration energy. For example, taking $\beta_{z1}=0.5714$, we have $\gamma_1=1.7782$ from Fig. 6; $\beta_{z2}=0.2878$ from Fig. 7; $\alpha_1=1.0460$ and $\alpha_2=2.6932$ from Fig. 8; $B_{01}=0.0989$ T and $B_{02}=0.1664$ from Fig. 9.

## IV. SIMULATION ANALYSIS

In this section, we will present simulation results on a CARA for the Yale gyroresonance harmonic converter. The CARA combines tapering a waveguide and tapering a magnetic field to keep the synchronous condition satisfied, as shown in Fig. 10. A 100-kV, 30-A, single-momentum electron beam is passed through the CARA driven at 2.856 GHz with an rf power of 10 MW. After the CARA, there is a drift tube to allow the beam to fulfill both the synchronous and grazing conditions as stated previously. The basic equations in this simulation are given in Sec. II. To save computer time, we use only five computational particles with an initial velocity ratio of $\alpha_0=0.0036$ ($u_{z0}=0.6555$) to simulate the beam, and the five particles are uniformly initialized in $\psi$ from $-3\pi/2$ to $\pi/2$.

In the 50.9-cm long CARA, there are three sections of waveguide. The first has a radius of 3.81 cm and a length of 11.53 cm, and the third has a radius of 5.08 cm and a length of 19.05 cm, and they are uniform. The second is tapered with a length of 20.32 cm.

First, we will simulate an electron beam passing through the CARA with an exact resonant magnetic field and through the drift tube with a transition magnetic field in order to examine the evolution of the beam. Then we will use a perturbed field, through deviations in the guide field from the resonant profile, to simulate the same beam and to observe how the perturbation affects the acceleration.

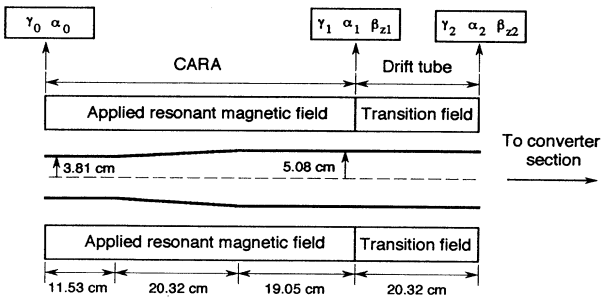


FIG. 10. CARA with a drift tube as used in simulations. The drift tube is used to transit the beam from CARA to the harmonic converter section.

### A. CARA with an exact resonant magnetic field

From Eq. (13) we see that an exact resonant magnetic field is dependent on the energy and axial velocity of individual moving electrons. The exact fields for different electrons are not completely the same because they have different initial conditions. In this simulation, we take an "exact" resonant magnetic field for all electrons in such a way that the synchronous condition is maintained for the first computational particle.

Figure 11 shows averaged transverse and axial velocities, and energy vs axial distance, where $\langle\ \rangle$ signifies the ensemble average. The transverse velocity $\langle\beta_\perp\rangle$ and energy $\langle\gamma\rangle$ increase with the axial distance $z$ while the axial velocity $\langle\beta_z\rangle$ does not change very much during the acceleration (from $z=0$ to 0.509 m). The resonant magnetic field $B_0$ gradually increases in the uniform waveguide and decreases a bit in the tapered waveguide. In the drift tube (from $z=0.509$ to 0.712 m), $B_0$ rapidly increases with axial distance, which results in considerable decrease in $\langle\beta_z\rangle$ and increase in $\langle\beta_\perp\rangle$ with $\langle\gamma\rangle$ kept unchanged. At the CARA exit, $\langle\beta_z\rangle=0.5714$, $\langle\gamma\rangle=1.7766$ (397 kV), and $B_0=0.0988$ T; after the drift tube, $\langle\beta_z\rangle=0.2923$, and $B_0=0.1658$ T. These results are very close to the ones obtained analytically in Sec. III. The CARA efficiency is 89.05% for this example.

Figure 12 shows rms spread in $\beta_\perp$, $\beta_z$, and $\gamma$. The $\beta_\perp$ spread has an abrupt peak nearly at start that can be explained as follows. At the CARA entrance, the beam of electrons does not have any velocity spread but a small transverse velocity. These electrons are in all directions, and some are accelerated and some are decelerated as soon as they go into the CARA, which results in a large increase in $\beta_\perp$ spread. However, all the electrons are forced to rapidly turn to the direction opposite to the rf field, and their transverse velocities get closer to their average when they are effectively accelerated. Accordingly, the $\beta_\perp$ spread begins to decrease. From this we can see that $\beta_\perp$ and $\gamma$ spreads during the acceleration result

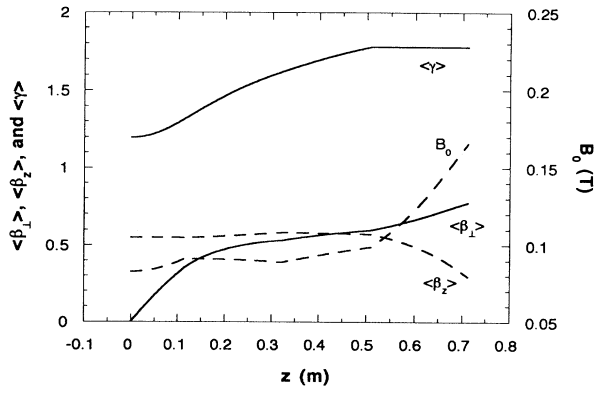


FIG. 11. Dependence of $\langle\beta_\perp\rangle$, $\langle\beta_z\rangle$, $\langle\gamma\rangle$, and exact resonant magnetic field $B_0$ on axial distance $z$ in the CARA (from $z=0$ to 0.509 m) and in the drift tube (from $z=0.509$ to 0.712 m). At the CARA exist, $\langle\beta_z\rangle=0.5714$, $\langle\gamma\rangle=1.7766$, and $B_0=0.0988$ T. After the drift tube, $\langle\beta_z\rangle=0.2923$, $B_0=0.1658$ T.

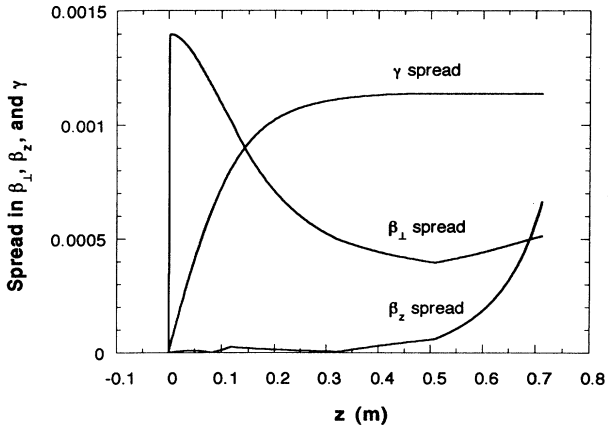


FIG. 12. Dependence of rms spread in $\beta_\perp$, $\beta_z$, and $\gamma$ on axial distance $z$. The $\gamma$ spread and $\beta_\perp$ spread result mainly from the beam's initial transverse velocity.

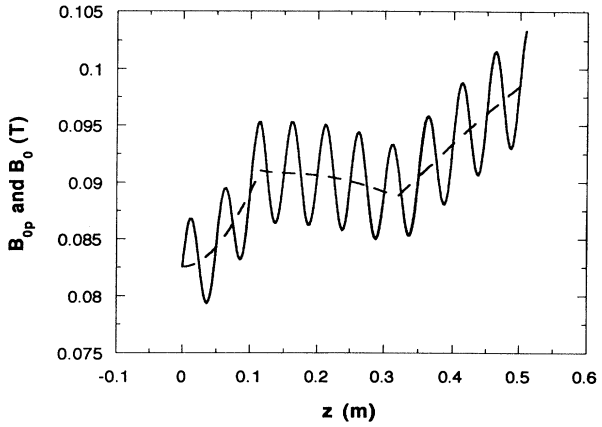


FIG. 14. Dependence of perturbed field $B_{0p}$ and exact resonant field $B_0$ on axial distance $z$. Solid line: 5% perturbation of the exact resonant field, and dashed line: exact resonant field.

mainly from the beam's initial transverse velocity. In the drift tube, the $\beta_z$ spread has a considerable increase because of $\gamma$ spread.

Figure 13 shows dependence of $\psi$ spread on axial distance. The five particles with an initial spread of $2\pi$ are strongly phase trapped as soon as they go into the CARA. The first two particles stay at $\psi=2\pi$ and the last three stay at $\psi=0$ with an extremely small $\psi$ spread (less than 0.03 rad). In the drift tube, the $\psi$ spread keeps almost unchanged although $\psi$ changes to fit the harmonic converter section.

### B. CARA with a perturbed magnetic field

To study deviations in the guide field from the exact resonant profile, we use the perturbed magnetic field $B_{0p}(z)=[1+\sigma\sin(2\pi z/\lambda_p)]B_0(z)$, where $\sigma=5\%$ is the perturbation coefficient, $\lambda_p=5$ cm is the perturbation period, and $B_0(z)$ denotes the exact resonant field, as shown in Fig. 14. Using this perturbed field, we have simulated the same electron beam passing through the CARA as in Sec. IV A.

Figure 15 shows dependence of relative frequency detuning $\Delta$ on axial distance $z$. For an exact resonant field, the maximum detuning is only about 0.1%, but for the perturbed field the maximum detuning increases up to about 6%. The perturbed field causes large deviations in the relative frequency detuning from the exact synchronous condition. However, the $\psi$ spread does not increase except for a little bumping (within $\pm 0.04$ rad), as shown in Fig. 16. Simulations indicate that the bumping magnitude increases with increase in the perturbation period. From Fig. 17, we find that the average transverse velocity $\langle\beta_\perp\rangle$ and axial velocity $\langle\beta_z\rangle$ also have some ripples, but the energy $\langle\gamma\rangle$ does not have any observable variations. At the CARA exit, $\langle\gamma\rangle=1.7755$, only 0.06% less than that in the exact resonant field case. This is because the electrons are so strongly trapped that the acceleration is

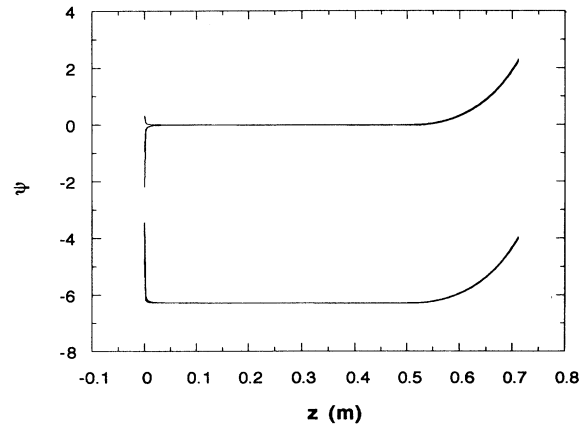


FIG. 13. Dependence of $\psi$ on $z$ for five computational particles, which are initially located at $\psi/\pi=-1.5$, $-1.1$, $-0.7$, $-0.3$, and 0.1. These particles are immediately phase trapped with an extremely small spread after they go into the CARA.

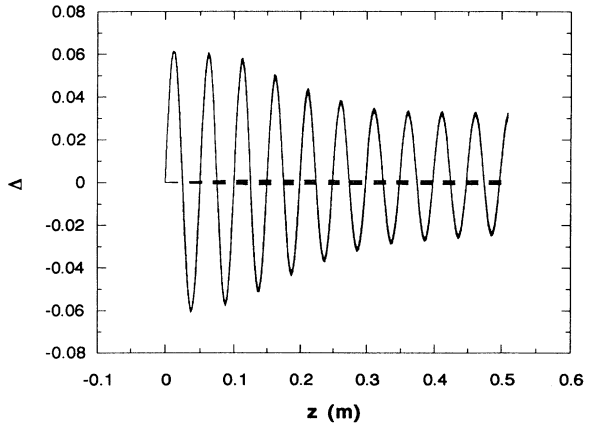


FIG. 15. Dependence of relative frequency detuning $\Delta$ on axial distance $z$ for five computational particles. Solid line: perturbed field, and dashed line: exact resonant field. $\Delta_{max}$ is only about 0.1% for the exact resonant field, and $\Delta_{max}$ increases up to about 6% for the perturbed field.

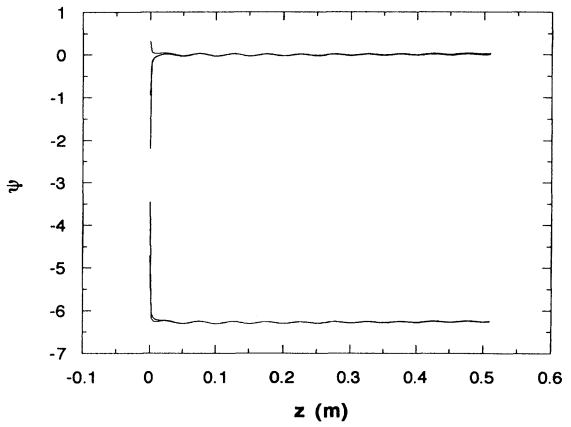


FIG. 16. Dependence of $\psi$ on $z$ for five particles in a perturbed magnetic field. The $\psi$ spread does not increase, compared with in the exact resonant field case, except for a little bumping.

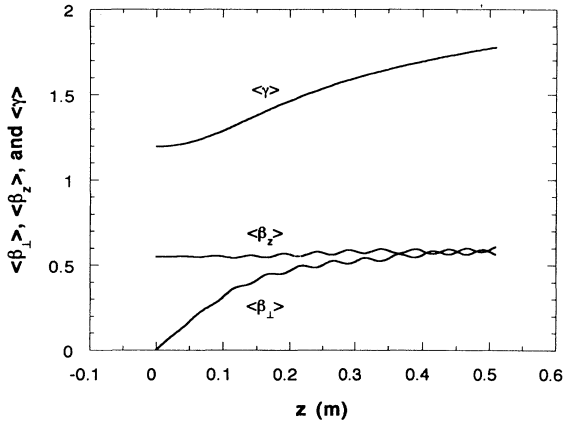


FIG. 17. Dependence of $\langle\beta_\perp\rangle$, $\langle\beta_z\rangle$, $\langle\gamma\rangle$ on axial distance $z$ in the CARA with a perturbed magnetic field. At the CARA exit, $\langle\gamma\rangle=1.7755$, only 0.06% less than that in the exact resonant field case.

not affected materially. Exploring this trapping phenomenon with other perturbation periods shows similar results, and no unusual resonance effect when $\lambda_p$ is close to the equilibrium orbit period.

## V. CONCLUSIONS

In this paper, based on a prior work [6], we have made an analytic study and computer simulation of CARA. In summary, we can draw the following conclusions:

(i) An approximate constant of the motion $u_\perp^2/b_0-2\gamma$ has been identified for an idealized $TE_{11}$-mode CARA. This constant has been previously applied to cyclotron resonance masers [8] and plasma heating [9,10]. In the case without an rf field, this constant of motion becomes the ordinary first adiabatic invariant.

(ii) An analytical expression for maximum acceleration energy in the CARA, $\gamma_{1\max}=\gamma_0+[(\gamma_0^2-1)/(1-n_1^2)]^{1/2}$ has been derived. The maximum acceleration energy depends only on the initial energy of an injected electron beam and the output waveguide refractive index.

(iii) There is a usable CARA upper energy limit for a gyroharmonic converter, given by $\gamma_{1\,\text{limit}}=\gamma_0+(\gamma_0^2-1)^{1/2}$. To fit the harmonic converter section, the energy of an electron beam prepared by the CARA must be less than the energy limit.

(iv) Simulations indicate that an electron beam is rapidly and strongly phase trapped in the CARA interaction. Even up to 6% of deviation in the relative frequency detuning from the exact synchronous condition does not materially affect the acceleration.

## ACKNOWLEDGMENTS

Helpful discussions with A. K. Ganguly, M. LaPointe, R. Yoder, and B. Hafizi are acknowledged. The work was supported by the Naval Research Laboratory and by the U.S. Department of Energy.

[1] J. L. Hirshfield, Phys. Rev. A **44**, 6845 (1991).
[2] J. L. Hirshfield, Phys. Rev. A **46**, 5161 (1992).
[3] A. K. Ganguly and J. L. Hirshfield, Phys. Rev. Lett. **70**, 291 (1993).
[4] A. K. Ganguly and J. L. Hirshfield, Phys. Rev. E **47**, 4364 (1993).
[5] C. Chen, Phys. Fluids **B 3**, 2933 (1991); Phys. Rev. A **46**, 6654 (1992).
[6] B. Hafizi, P. Sprangle, and J. L. Hirshfield, Phys. Rev. E **50**, 3077 (1994).
[7] L. Friedland, Phys. Plasmas **1**, 421 (1994).
[8] G. S. Nusinovich, Phys. Fluids **B4**, 1989 (1992); P. E. Latham and G. S. Nusinovich, in *Advanced Accelerator Concepts,* edited by J. S. Wurtele, AIP Conf. Proc. No. 279 (AIP, New York, 1992), pp. 42–55.
[9] B. Hafizi and R. E. Aamodt, Phys. Fluids **30**, 3059 (1987).
[10] V. A. Zhil'tsov, A. A. Skovoroda, A. V. Timofeev, K. Yu. Kharitonov, and A. G. Shcherbakov, Fiz. Plasmy **17**, 771 (1991) [Sov. J. Plasma Phys. **17**, 447 (1991)].
[11] V. S. Voronin and V. K. Kononov, Zh. Tekh. Fiz. **40**, 160 (1970) [Sov. Phys. Tech. Phys. **15**, 115 (1971)].